# A strategy for the estimation of the fatigue life of notched components under random multaxial fatigue

**G. Cailletaud[1], T. Herbland[1], B. Melnikov[2], A. Musienko[2], S. Quilici[1]**

[1]MINES ParisTech, Centre des Matériaux, CNRS UMR 7633,
BP 87, 91003 Evry Cedex, France

[2]State Polytechnical University, Material Strength Department,
195251 St-Petersburg, Russia

***ABSTRACT*** *This paper describes three new models that can be used (1) to determine the stress–strain response in stress concentration zones for components submitted to complex multiaxial loading paths, (2) to extract relevant cycle sequences from a general three-dimensional loadin path, (3) to find the hypersphere enclosing any type of cyclic load history. These three models can be combined to post-process an elastic Finite Element Analysis, and provide a fast estimation of the fatigue life of the components.*

## 1 INTRODUCTION

The application of multiaxial random loadings on notched components generates complex stress and strain histories at the notch root. This can be modelled by means of Finite Element Analyses (FEA), nevertheless, there is also a need for simplified approaches in order to perform fast computations of the component life. A global strategy must first provide a stress–strain history on critical points, then apply a post-processing to extract cycles from the complex signal, and finally use a fatigue model to compute the number of cycles to failure. The present paper is focused on the second part of the chain. It describes a multiaxial rainflow technique able to extract a series of cycles from a prescribed three-dimensional stress history. This method uses a specific solution to place an hypersphere around a given number of points in the stress space, that is described as well.

## 2 AN ELASTOPLASTIC CORRECTION IN STRESS CONCENTRATION ZONES

This part of the strategy is just recalled here for the sake of completeness. A full description of the method is provided in a recently submitted paper [1]. Its development started from the observation that classical models like Neuber's [2] or generalized Neuber rules [3–7] hardly account for the minor components in the case of three-dimensional

loadings. This can be easily illustrated by the example of an axisymmetrical notched specimen loaded in tension. Eight unknowns have to be introduced to characterize notch root behaviour. Namely, in cylindrical coordinates where $(r,z,\theta) \equiv (1,2,3)$, one has two non zero stress components ($\sigma_2$ and $\sigma_3$), three non zero strain (plastic strain) components, ($\varepsilon_1$, $\varepsilon_2$, $\varepsilon_3$)/($\varepsilon_1^p$, $\varepsilon_2^p$, $\varepsilon_3^p$). The equations available to solve the problem are three non trivial elasticity relations, three non trivial equations provided by the plasticity model. Two more equations are then needed. One of them is given by a scalar rule involving strain$\times$stress terms (like $\sigma_{ij}\varepsilon_{ij}$), that characterizes flow *intensity*. The last one must define the relative amount of plasticity on each component, thus the flow *direction*. The consequence of such an approach is that the applicability of the various rules are restricted to a narrow domain, not far from the identification conditions.

The proposed approach uses an adaptative correction technique, that introduces adjustable parameters to build an estimation of the elastoplastic solution from the elastic field. The local field is obtained by using a concentration rule, that provides the stress tensor for an elastoplastic behaviour, $\underset{\sim}{\sigma}$, by substracting a corrective term to the stress tensor originating from the elastic computation, $\underset{\sim}{\sigma}^e$:

$$\underset{\sim}{\sigma} = \underset{\sim}{\sigma}^e - \underset{\approx}{C} : \underset{\sim}{\beta} \tag{1}$$

The tensorial variable $\underset{\sim}{\beta}$ is a function of the local plastic strain $\underset{\sim}{\varepsilon}^p$. Its rate is defined as

$$\dot{\underset{\sim}{\beta}} = \dot{\underset{\sim}{\varepsilon}}^p - \underset{\approx}{D} : \left( \underset{\sim}{\beta} - \underset{\approx}{\delta} : \underset{\sim}{\varepsilon}^p \right) ||\dot{\underset{\sim}{\varepsilon}}^p|| \tag{2}$$

When applied to axisymmetrical notched specimens, these relations provide the two missing equations that close the problem. Two cases have been considered:

- linear corrective term, $\underset{\approx}{C} = \underset{\approx}{C}^L$ and $\underset{\approx}{D} = 0$;
- non linear corrective term, $\underset{\approx}{C} = \underset{\approx}{C}^N$ and $\underset{\approx}{D} = \underset{\approx}{D}^N$;

The tensor $\underset{\approx}{\delta}$ depends on one parameter only, since $\underset{\approx}{\delta} = \delta$ `diag` (1,1,1,1/2,1/2,1/2), meanwhile $\underset{\approx}{C}$ and $\underset{\approx}{D}$ are symmetric fourth order tensors that ensure a zero stress vector at the free surface. In Voigt notation, assuming that $x_1$ is normal to the surface, only the terms 22, 23, 33 and 55 are non zero. These non-zero components are calibrated by means of an optimization process where the output of the simplified model is compared to the result of a finite element analysis. After identification, the model is able to represent any type of loading. It has already been used for notched specimens submitted to complex non proportional tension-torsion loading paths [1].

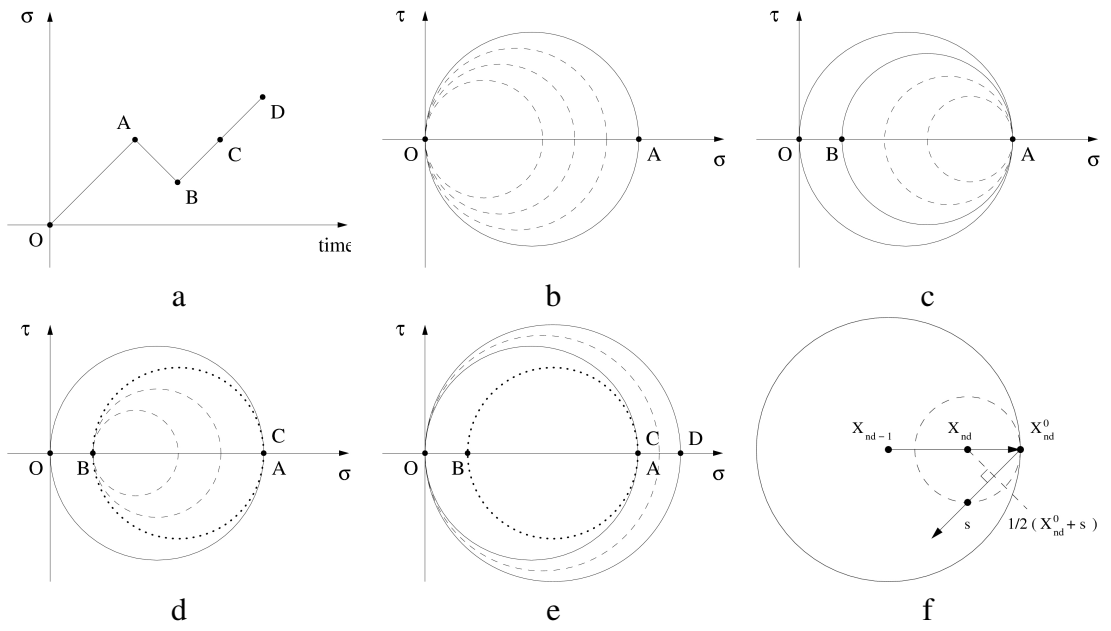


Figure 1: Illustration of the cycle extraction procedure: (a) Example of a one dimensional loading path; (b) Successive locations (dashed circles) of the domain circumscribing the loading path during the first loading OA and final position (solid circle); (c) Successive locations and final domains during AB branch (d) Successive locations and final domains during BC branch (e) Elimination of the circle of diameter AB and growth of the former OA diameter circle to reach OD. (f) Determination of the center of the current active surface for a non-proportional loading [9]

## 3 A MULTIAXIAL RAINFLOW ALGORITHM

The algorithm is based on the "active surface" concept used in some plasticity models. Its first version was developed by Melnikov and Semenov [8]. Like onedimensional rainflow technique, it provides a series of centers and ranges coming from the extracted cycles, but instead of working on one dimension, the algorithm accounts for the full tensorial form. The various steps of the method are explained in figure 1, for the elementary case of a cyclic tensile load (Fig.1a). The purpose is to dynamically generate surfaces that include a part of the loading path. The algorithm starts with an initial surface reduced to a point at the origin, 0. Along the OA branch, the surface diameter is defined by O and the current point, ending at OA (Fig.1b). Just after A, an unloading is detected, and a new surface is created inside the first one. During the AB branch, it grows until B (figure 1 (c)). Again, an unloading is detected after B and a third surface is created, which grows until C (Fig.1d). Once the current point reaches C, the second and the third active surfaces coincide, that means that one cycle is closed. It is then extracted (Fig.1d). As a result, the first surface becomes active again and grows until D (Fig.1e).

Unloadings are rather easy to detect in the onedimensional case. In more complex

cases, a criterion is needed. Assuming that a solid-line surface defined by its center $\underset{\sim}{\mathbf{X}}_{n-1}$ and its radius $R$ has been created, the unloading condition writes (Fig.1f):

$$(\underset{\approx}{\mathbf{s}} - \underset{\approx}{\mathbf{X}}_{n-1}) : d\underset{\approx}{\mathbf{s}} < 0 \tag{3}$$

When unloading is detected, the origin $\underset{\sim}{\mathbf{X}}_n^0$ of the new active surface is saved. Then, the center $\underset{\sim}{\mathbf{X}}_n$ of this surface moves between $\underset{\sim}{\mathbf{X}}_n^0$ and the center of the former active surface $\underset{\sim}{\mathbf{X}}_{n-1}$. This center is the intersection of the right bissector of ($S$,$X_n^0$) at point $\frac{1}{2}\left(X_n^0 + s\right)$ with the straight line ($X_{n-1}$,$X_n^0$). This simple rule fails in two cases:

- It overestimates the external cycle amplitude when applied to a loading path such that more than two points lie on the surface. This is illustrated for instance with an equilateral triangle-shaped load path, ABC, the origin being point A. The extracted surface has a radius AB, and remain centered in A, instead of having a center at the centroid of the triangle, $X^*$.

- A problem appears when the unloading direction is almost orthogonal to the previous one (i.e. if ($X_n^0$ $S$) and ($X_{n-1}$ $X_n^0$) would be orthogonal in figure 1f). The new surface is too big again, and the external cycle is overestimated.

The first problem can be solved by a preliminary determination of the external cycle, by means of an algorithm presented in section 4. The rainflow process is then initialized at $X^*$. The second one is avoided by neglecting unloadings whose intensity is too small (in terms of variation of von Mises equivalent).

## 4 THE SMALLEST ENCLOSING HYPERSPHERE TO A MULTIAXIAL LOAD PATH

The algorithm presented in this section aims at finding the amplitude $\Delta J$ of a multiaxial load path $P = \left\{\underset{\sim}{\sigma}_i\ ,\ i = 1,s\right\}$, where $s$ is the number of points in the path. Calculation of $\Delta J$ is a key problem in many fatigue multiaxial models and is also used as initialization for the multiaxial rainflow procedure. The only satisfying way to define $\Delta J$ is to find the so-called "smallest enclosing hypersphere" (SEH problem), that contains all points of $P$. In the general 3D case, $\underset{\sim}{\sigma}$ is 2nd order symmetric tensor with 6 independent components. The smallest hypersphere is thus sought in a space with dimension $d = 6$, the measure of distance used in this space being the von Mises stress invariant $J_2(\underset{\sim}{\sigma})$. This problem was investigated by many authors during the last decades. One of the most efficient methods was developed by Welzl [10], improved by Gaertner [11]. The other existing methods are summarized by Bernasconi and Papadopoulos [12]. In the latter case, the search is limited to finding the shear amplitude on a critical plane (2D search only), and an exhaustive search was initially proposed: calculate the radius of circles built on all couples and triplets of points in $P$ (if the they do define a circle), the maximum of those is $\Delta J$.

This brute-force method is computationally unmanageable as soon as the size of $P$ becomes large, or even for small sets in the general 3D case, where the calculation should

**a) Exhaustive search($P$)**

p=2
**while** $p \leqslant c+1$
  **for** each p-uplet $C$ of P
    **if** $C$ defines an hypersphere $H$ **then**
      **check** if $H$ encloses all points of $P$
      **if** true **then** $\Delta\sigma$ = radius of $H$ , **end**
  $p = p+1$

**b) Optimization problem** $O(P)$

Find the center $\underset{\sim}{\mathbf{X}}$ of $H$ with radius $R(\underset{\sim}{\mathbf{X}})$:

$\underset{\underset{\sim}{\mathbf{X}}}{Min}\ \left\{R(\underset{\sim}{\mathbf{X}})\right\}$

with constraints:

$J_2(\underset{\sim}{\sigma}_i, \underset{\sim}{\mathbf{X}}) \leqslant R(\underset{\sim}{\mathbf{X}})\ ,\ \underset{\sim}{\sigma}_i \in P\ \ (i = 1,s)$

where $R(\underset{\sim}{\mathbf{X}}) = \underset{i}{Max}\left\{J_2(\underset{\sim}{\sigma}_i - \underset{\sim}{\mathbf{X}})\right\}$

Figure 2: Conventional methods used to solve the SEH problem in a $c$-dimensional space

involve all possible p-uplets ($p \leqslant 7$) in set $P$. In the 3D case, using the fact that the problem has indeed an unique solution, a slightly improved exhaustive search procedure could be summarized as shown in figure 2a.

Alternatively, the SEH problem can be redefined as a constrained optimization problem (Fig.2b). $O(P)$ is a well-defined convex optimization problem that can be solved by classical methods such as the SQP algorithm. This approach has been used by some authors for pattern classification applications [13]. In our case, for this key step in fatigue life evaluation procedures, we prefer not to rely on a numerical method that may fail to converge to the required accuracy. An original algorithm that is designed to give the *exact* solution of $O(P)$ in a minimum number of iteration is then proposed hereafter.

Let's first suppose that we already know a point $\underset{\sim}{\sigma}^*$ on the optimal hypersphere, a new optimization problem $O_{\underset{\sim}{\sigma}^*}(P)$, more convenient for numerical treatment, can be defined as follows:

Find the center $\underset{\sim}{\mathbf{X}}$ of the minimum sphere passing through $\underset{\sim}{\sigma}^*$ and enclosing all points of $P$:

$\underset{\underset{\sim}{\mathbf{X}}}{Min}\ \left\{J_2(\underset{\sim}{\sigma}^* - \underset{\sim}{\mathbf{X}})\right\}$ with constraints: $J_2(\underset{\sim}{\sigma}_i, \underset{\sim}{\mathbf{X}}) \leqslant J_2(\underset{\sim}{\sigma}^*, \underset{\sim}{\mathbf{X}})\ ,\ i = 1,s\ ,\ \underset{\sim}{\sigma}_i \neq \underset{\sim}{\sigma}^*$

Following a classical technique, we can convert $O_{\underset{\sim}{\sigma}^*}(P)$ to an unconstrained dual problem:

$$\underset{\lambda_i \geq 0\,,\,\underset{\sim}{\sigma}_i \neq \underset{\sim}{\sigma}^*}{Max}\ \ \underset{\underset{\sim}{\mathbf{X}}}{Min}\ L(\underset{\sim}{\mathbf{X}}, \lambda_i)$$

with $L(\underset{\sim}{\mathbf{X}}, \lambda_i) = \left[J_2(\underset{\sim}{\sigma}^* - \underset{\sim}{\mathbf{X}}) + \lambda_i \left(J_2(\underset{\sim}{\sigma}_i - \underset{\sim}{\mathbf{X}}) - J_2(\underset{\sim}{\sigma}^* - \underset{\sim}{\mathbf{X}})\right)\right]$ the lagrangian function, and $\lambda_i$ Lagrange multipliers associated to constraints of $O_{\underset{\sim}{\sigma}^*}(P)$.

The Kuhn–Tucker conditions for the optimum define a linear system with unknowns $\lambda_i$, that can be solved by a standard direct solver (a method able to handle singular systems is needed here) to find the exact solution of $O_{\underset{\sim}{\sigma}^*}(P)$. Solution $\underset{\sim}{\mathbf{X}}$ for the center of the optimal hypersphere can then be calculated from the $\lambda_i$ by: $\underset{\sim}{\mathbf{X}} = \underset{\sim}{\sigma}^* + \underset{i\,,\,\underset{\sim}{\sigma}_i \neq \underset{\sim}{\sigma}^*}{\sum} \lambda_i (\underset{\sim}{\sigma}_i - \underset{\sim}{\sigma}^*)$

When solving the linear system for the $\lambda_i$, several cases can happen: if $\lambda_i > 0$: the point $\underset{\sim}{\sigma}_i$ is on the optimal sphere, if $\lambda_i = 0$: the point $\underset{\sim}{\sigma}_i$ is inside the sphere, if $\lambda_i < 0$: the problem $O_{\underset{\sim}{\sigma}^*}(P)$ has no solution (ie. $\underset{\sim}{\sigma}^*$ is not on the optimal sphere).

Defining by $F(\underset{\sim}{\sigma})$ the point of $P$ whose distance to $\underset{\sim}{\sigma}$ is maximal, the algorithm proposed in this paper then consists to iteratively solve $O_{\underset{\sim}{\sigma}^*}(S)$ problems on subsets $S$ of $P$ in the following way (see also figure 3):

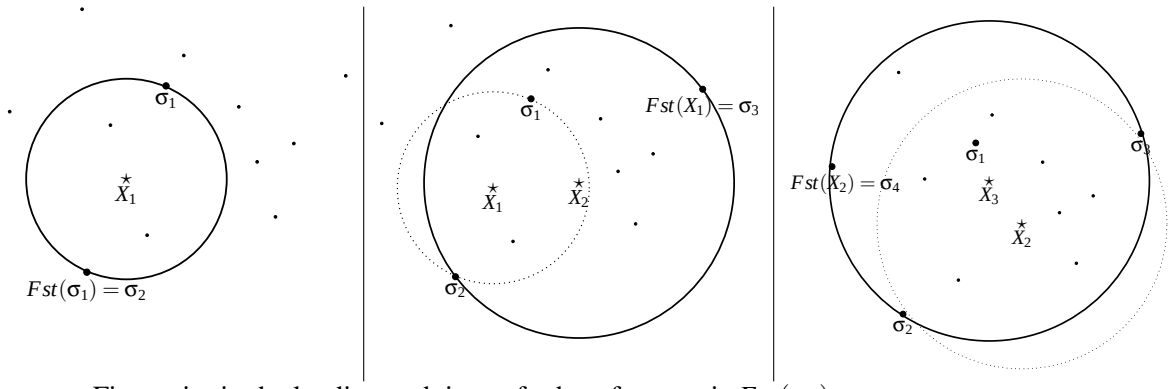


• First point in the loading path is $\sigma_1$, farthest from $\sigma_1$ is $Fst(\sigma_1) = \sigma_2$
• Iter 1: $S = \{\sigma_1, \sigma_2\}$ , $\sigma^* = \sigma_2$, solution is circle $H1$ with center $X_1$ , farthest from $X_1$ is $\sigma_3$ outside of $H1$
• Iter 2: $S = \{\sigma_1, \sigma_2, \sigma_3\}$ , $\sigma^* = \sigma_3$, solution is circle $H2$ with center $X_2$ , farthest from $X_2$ is $\sigma_4$ outside of $H2$
• Iter 3: $S = \{\sigma_1, \sigma_2, \sigma_3, \sigma_4\}$ , $\sigma^* = \sigma_4$, solution is circle $H3$ with center $X_3$ , all points of $P$ are inside H1, **end**

Figure 3: Iterations needed by the MHA algorithm in a biaxial case

**Minimum Hypersphere Algorithm (MHA)**
initialization: $\underset{\sim}{\sigma}^* = F(\underset{\sim}{\sigma}_1)$ , initial subset $S = \left\{ \underset{\sim}{\sigma}_1 , F(\underset{\sim}{\sigma}_1) \right\}$
**while** not found **do**
a) **solve** $O_{\underset{\sim}{\sigma}^*}(S)$ on subset $S$
**if** no solution ($\lambda_i < 0$) do **Exhaustive search**($S$) on subset $S$
(in either case a smallest sphere $H$ with center $\underset{\sim}{\mathbf{X}}$ enclosing $S$ is found at this point)
**check** if $H$ contains all points of $P$
**if** true **then** $H$ is the optimal solution , **goto** end
b) Heuristic choice to expand subset $S$
**find** $F(\underset{\sim}{\mathbf{X}})$ the point at a maximal distance from the center $\underset{\sim}{\mathbf{X}}$ of $H$
$S = S \cup \left\{ F(\underset{\sim}{\mathbf{X}}) \right\}$ , $\underset{\sim}{\sigma}^* = F(\underset{\sim}{\mathbf{X}})$ , **goto** a)

Experience shows that even on very large load paths (the algorithm has been applied to stochastic stress evolutions coming from car damping systems measurements where the size of $P$ exceed $10^5$ points), this algorithm quickly converge (in general less than 10 iterations are necessary) to the optimal solution. The heuristic used at each step for the choice of $\underset{\sim}{\sigma}^*$ is also very efficient: $O_{\underset{\sim}{\sigma}^*}(S)$ has generally a solution, and an exhaustive search on $S$ is therefore scarcely needed. Note however that an exhaustive search, if needed, is performed only on a very small subset of $P$ (size of the subset is $i+1$, with $i$ the number of iterations).

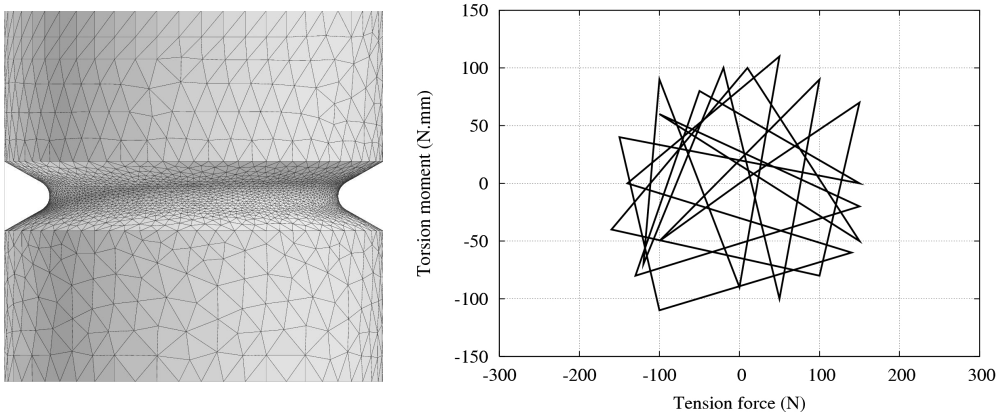


Figure 4: Axisymmetric notched specimen in tension–torsion. (a) FE mesh (60905 elements, 267807 dof); (b) The random tension–torsion loading path

## 5 APPLICATION AND CONCLUDING REMARKS

The method is applied to an axisymmetric notched specimen submitted to a complex tension–torsion loading, as shown in figure 4. A non linear correction is introduced, with $\delta = 0.92$, and the following values for the components of $\underset{\approx}{C}$ and $\underset{\approx}{D}$:

| | | | |
|---|---|---|---|
| $C^N_{22} = 1.22.10^5$ MPa | $C^N_{33} = 2.14.10^5$ MPa | $C^N_{23} = 4.02.10^4$ MPa | $C^N_{55} = 6.17.10^4$ MPa |
| $D^N_{22} = 1.45.10^1$ | $D^N_{33} = 7.72.10^2$ | $D^N_{23} = 6.64.10^1$ | $D^N_{55} = 3.81.10^2$ |

The resulting local stress history is illustrated in figure 5, that shows first the components 22, 33, and 23 (respectively Fig.5a,b,c). The agreement with the finite element solution is excellent. Note that the corrective parameters were identified on one hand in tension only, on the other hand in torsion only, and that the same parameters were used for a complex loading. The accumulation of plasticity is also well represented (see Fig.5d).

The three models can be seen as building bricks of a general purpose suite that can account for any kind of three-dimensional fatigue loading and generate robust life estimations even for complex loading paths [14].

## REFERENCES

[1] Herbland, T., Quilici, S., and Cailletaud, G. (2010) *submitted*.

[2] Neuber, H. (1961) *J. of Applied Mechanics* **28**, 544–551.

[3] Chaudonneret, M. and Culié, J. (1985) *La Recherche Aérospatiale* **4**, 33–40.

[4] Hoffmann, M. and Seeger, T. (1985) *J. of Engng. Mat. Technol.* **107**, 250–254.

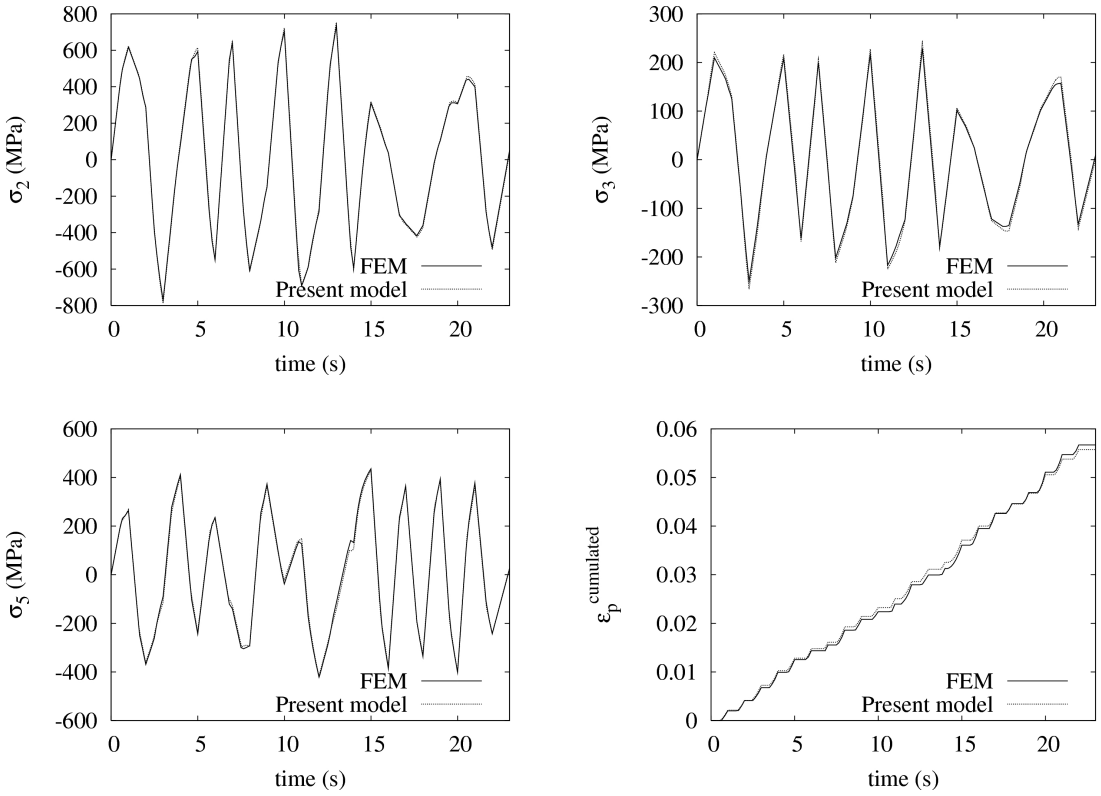


Figure 5: Comparison of the local histories obtained by FEA and the present model for a random non-proportional loading

[5] Barkey, M., Socie, D., and Hsia, K. (1994) *J. of Engng. Mat. Technol.* **116**, 173–180.

[6] Desmorat, R. (2002) *Int. J. Solids Structures* **39**, 3289–3310.

[7] Buczynski, A. and Glinka, G. (2003) *Biax./Multiax. Fatigue and Fracture* , 265–283.

[8] Melnikov, B. and Semenov, A. (1998) *Zeit. angew. Math. und Mech.* **78**, 615–616.

[9] Quilici, S. and Musienko, A. Tech.report ARMINES - MINES ParisTech Oct. 2004.

[10] Welzl, E. (1991) *New Results and New Trends in Computer Science* **555**, 359–370.

[11] Gärtner, B. (1999) *Lecture Notes in Computer Science* **1643**, 693.

[12] Bernasconi, A. and Papadopoulos, I. (2005) *Comput. Mat. Sci.* **34**, 355–368.

[13] Wang, J., Neskovic, P., and Cooper, L. (2007) *Neurocomputing* **70(4-6)**, 801–808.

[14] http://www.mat.ensmp.fr/Recherche/Valorisation/fr_zebulon.php.